Separation Science and Technology
Publication details, including instructions for authors and subscription information:
http://www.informaworld.com/smpp/title~content=t713708471

Solvent Vapor Recovery by Pressure Swing Adsorption. I. Experimental Transient and Periodic Dynamics of the Butane-Activated Carbon System

Yujun Liu; Charles E. Holland; James A. Ritter

To cite this Article Liu, Yujun , Holland, Charles E. and Ritter, James A.(1998) 'Solvent Vapor Recovery by Pressure Swing Adsorption. I. Experimental Transient and Periodic Dynamics of the Butane-Activated Carbon System', Separation Science and Technology, 33: 15, 2311 — 2334
To link to this Article: DOI: 10.1080/01496399808545277
URL: http://dx.doi.org/10.1080/01496399808545277

SEPARATION SCIENCE AND TECHNOLOGY, 33(15), pp. 2311–2334, 1998

Solvent Vapor Recovery by Pressure Swing Adsorption. I. Experimental Transient and Periodic Dynamics of the Butane–Activated Carbon System

YUJUN LIU, CHARLES E. HOLLAND, and JAMES A. RITTER*
DEPARTMENT OF CHEMICAL ENGINEERING
SWEARINGEN ENGINEERING CENTER
UNIVERSITY OF SOUTH CAROLINA
COLUMBIA, SOUTH CAROLINA 29208, USA
TELEPHONE: (803) 777-3590
FAX: (803) 777-8265
E-MAIL: ritter@sun.che.sc.edu

ABSTRACT

An experimental investigation was carried out for the separation and recovery of butane vapor (10 to 40 vol%) from nitrogen using Westvaco BAX activated carbon in a twin-bed pressure swing adsorption (PSA) system utilizing a 4-step Skarstrom-type cycle. Twenty-four runs, covering a broad range of process and initial column conditions, were performed to investigate the transient and periodic process dynamics. In all cases the approach to the periodic state was very slow, taking up to 160 cycles depending on the initial condition of the beds; and peak bed temperatures of up to 105°C were observed depending on both the initial condition of the beds and the process conditions. Also, the periodic state of each run was unique when approaching a new periodic state from less contaminated beds. The uniqueness of the periodic states, together with the exceedingly high peak temperatures, inferred much about the practice of preconditioning beds to avoid high temperature excursions. The periodic enriched butane vapor concentration histories also gave considerable insight into new cycle designs for improved solvent vapor enrichment.

INTRODUCTION

The conventional pressure swing adsorption (PSA) process, i.e., PSA for purification and separation, has been studied extensively during the past two

* To whom correspondence should be addressed.

decades (1–4). PSA for solvent vapor recovery (SVR) has also been receiving attention since its recent commercialization (5–13). However, even for the conventional PSA purification and separation processes, most of the published literature has focused only on the periodic state performance; transient and periodic dynamics have rarely been reported. Yet the transient and periodic dynamics are indispensable to optimizing and designing PSA processes, especially with respect to verifying process simulation codes. Moreover, the transient process behavior of a PSA–SVR process is expected to be much different from the periodic behavior, especially the transient thermal behavior, because of the high affinity between the solvent vapor and adsorbent which gives rise to a large heat of adsorption.

Transient dynamics were reported by Ritter and Yang (7) in their PSA air purification study on the removal of dimethyl methylphosphomate (DMMP) vapor from air; simulated transient DMMP concentration profiles were reported for runs starting from clean and saturated beds. Kikkinides and Yang (14) discussed very briefly the simulated transient concentration profiles of SO_2 in an isothermal PSA process for SO_2/NO_x removal. Friday and LeVan (15) presented the transient behavior of the PSA-air purification system, but also under isothermal conditions. Kikkinides et al. (16) used a nonisothermal model to investigate the feasibility of natural gas desulfurization by a PSA process and showed some transient concentration profiles in the interest of studying the multiplicity of the periodic state; no transient temperature profiles were reported, however. Transient concentration and temperature profiles were reported by Chihara and Suzuki (17) for the PSA–air drying system and transient thermal effects were investigated by Psaras et al. (18) using a zeolite-filled single-bed PSA process where different gases were used to provide data on the effects of the heat of adsorption.

Periodic state dynamics were reported by Ruthven and Farooq (19) in terms of the effluent concentration histories in a cryogenic PSA process for concentrating traces of hydrogen/tritium from a helium carrier. The periodic state light product concentration histories were reported by Ritter and Yang (7) for the DMMP–air–PSA system, showing the effects of three process parameters, i.e., the purge-to-feed ratio, the pressure ratio, and the feed concentration. Besides the transient thermal behavior, Psaras et al. (18) also reported the periodic state thermal behavior in their model PSA processes. Yang and Doong (20) reported the periodic state effluent concentration histories in a five-step activated carbon PSA H_2/CH_4 separation process, where the effects of the purge-to-feed ratio, cocurrent depressurization, feed rate, and high pressure on the effluent histories were shown, along with typical temperature histories. The same kind of periodic information was also reported by Yang and coworkers in PSA bulk separations for H_2/CH_4 by 5A zeolite (21), H_2/CO by activated carbon (22) and 5A zeolite (23), $H_2/CH_4/CO_2$ by activated

carbon (24), $H_2/CH_4/H_2S$ by activated carbon (25), and $H_2/CH_4/CO/CO_2/H_2S$ by activated carbon (26). For the PSA–SVR process a relatively comprehensive study on the periodic process dynamics was performed by Liu and Ritter (11), where the periodic behavior of all the dependent variables (i.e., gas-phase concentration, temperature, loading and gas-phase velocity) were reported for the computer simulation of the PSA–benzene vapor recovery process.

In light of the limited information available on transient and periodic PSA process dynamics, especially for the PSA–SVR process, the objective of this study was to carry out a first-time experimental investigation of an actual PSA–SVR process at the bench-scale. The recovery of *n*-butane vapor from nitrogen-using Westvaco BAX activated carbon was chosen because of its commercial relevance. It represents one of the lighter components escaping from the liquid phase during the bulk transfer of gasoline from storage vessels (27). In this paper (Part I), the PSA system is described, and unique features of transient and periodic dynamic behavior are reported. In Part II of this study (28), the periodic performance of this process is reported.

EXPERIMENTAL

PSA Process Description

The PSA cycle utilized in this study was a Skarstrom-type cycle. During each cycle, two beds each underwent four steps, namely, (I) pressurization, (II) adsorption, (III) blowdown, and (IV) purge. While one bed was undergoing adsorption, the other bed was being purged, and while one bed was undergoing repressurization, the other bed was being depressurized. In this way the beds operated 180° out-of-phase with each other. During the adsorption step the gas mixture (butane/nitrogen) was fed into the bed at a constant high pressure, and the less selectively adsorbed component (nitrogen) was withdrawn as the light product. During the blowdown step the bed pressure was decreased from the high pressure to the low pressure by withdrawing gas through the feed end of the bed (countercurrent). The light product end of the bed was kept closed during this step. During the purge step the bed was countercurrently purged at the low pressure using the purified light product from the other bed undergoing the adsorption step. The gas enriched in the more selectively adsorbed component was withdrawn through the feed end during the blowdown and purge steps. During the pressurization step the bed pressure was increased from the low pressure to the high pressure by introducing fresh carrier gas (nitrogen) through the light product end (countercurrent) while keeping the feed end of the bed closed. At the end of this step the feed end was opened to begin the adsorption step of the next cycle. These coupled beds eventually reached a periodic state where the time-dependent

bed profiles and effluent concentration histories were reproduced from cycle to cycle.

Apparatus

A schematic of the PSA experimental system is displayed in Fig. 1. The 7.75-cm diameter (ID) by 30.48 cm long columns were each loaded with 430 g of dry BAX carbon. The adsorbent bed was held in place by two supported screens placed 1.67 cm from the top and bottom of the column. This made

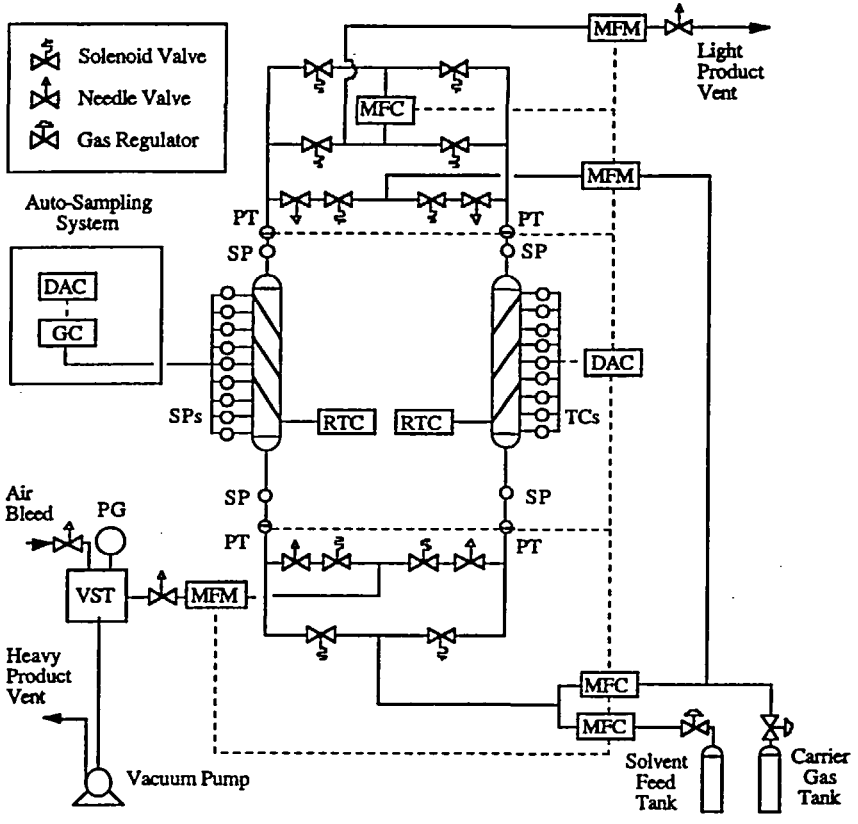

FIG. 1 Schematic of the *n*-butane–nitrogen–BAX carbon PSA–SVR system. DAC: data acquisition and control system; GC: gas chromatograph; MFC: mass flow controller; MFM: mass flowmeter; PG: pressure gauge; PT: pressure transducer; RTC: regeneration temperature controller; SP: sampling port; TC: thermocouple; VST: vacuum surge tank.

TABLE 1
Bed Characteristics of the Twin Bed PSA-SVR Apparatus[a]

Bed radius	0.0387 m
Bed length (L)	0.2724 m
Packing void fraction	0.391
Pellet density	550.0 kg/m^3
Pellet radius	0.00105 m
Adsorbent bed loading	430.0 g

[a] Additional characteristics are given in the text.

the actual adsorbent bed length equal to 27.14 cm. Additional characteristics of the bed are given in Table 1. Key mechanical features of this PSA–SVR system included three mass flowmeters (MFM), three mass flow controllers (MFC), four pressure transducers (PT), ten two-way solenoid valves, six needle valves, nine sample taps in one column, nine unsheathed thermocouples (TCs) in the other column, a high capacity vacuum pump, a vacuum surge tank (VST), and a gas chromatograph (GC) equipped with a thermal conductivity detector (TCD), and a computer-controlled integrator.

The nine sample taps in one of the columns were equally spaced at 2.86 cm along the length of the column. The first sample tap was located 2.19 cm from the bottom of the adsorbent bed, whereas the ninth sample tap was located 2.09 cm from the top of the adsorbent bed. The nine thermocouples in the other column were placed in exactly the same axial arrangement as the sample taps. Moreover, the exposed tip of each thermocouple was inserted exactly into the center of the bed to obtain the center line temperature profile.

Another key feature of this system was the National Instruments data acquisition and control (DAC) system. The DAC system controlled the solenoid valve operations, cycle time sequencing and mass flow controllers, and monitored the thermocouples, pressure transducers, mass flow meters, and cycle sequencing and number of cycles. The DAC system also controlled the autosampling system, which was used to measure the concentration profiles inside the bed. This sampling system consisted of nine microvolume solenoid values (one for each sample tap), vacuum and vent microvolume solenoid values for precleaning the sample loops, nine 5 cm^3 sample storage loops, a ten-point switching valve for sample tap selection, one additional 0.25 cm^3 global sample loop, and a multiport switching valve to send the sample stored in the global loop to the GC. This DAC system thus allowed for automatic mapping of temperature, pressure, and concentration profiles and histories within the columns.

Experimental Procedure

Initially, both beds were regenerated at 135 ± 15°C for 16 hours using a nitrogen purge under vacuum. The nitrogen purge was approximately 0.125 SLPM through each bed, and the vacuum level was approximately 3 kPa. For each series of runs, corresponding to the study of a particular parameter, the PSA process was initiated with completely regenerated beds cooled to room temperature and blanketed with nitrogen. Also, for each series of runs, the parameter of interest was set first at a value corresponding to the smallest bed penetration. All other process variables were fixed. Once the periodic state was reached, the value of this parameter was changed to the next value without stopping the process, and the system was allowed to reach the new periodic state. In this way a series of runs were continuously carried out where the bed become progressively more contaminated with each run.

During each run the butane/nitrogen feed and purge gas flow rates were controlled by the mass flow controllers. The light product and pressurization nitrogen gas flow rates, and the effluent flow rates during the blowdown and purge steps were measured continuously by the mass flowmeters. The high pressure was controlled using a needle valve located at the exit of the light product stream. Similarly, the low (vacuum) pressure was controlled using a needle valve located at the exit of the heavy product stream, in conjunction with a bleed valve used to control the vacuum level in the vacuum surge tank. The pressurization and blowdown rates were controlled and balanced for each bed using four needle valves, two valves for each bed. The pressure histories were measured by the pressure transducers placed at the bottom of each bed. All of this information was recorded through the DAC system, and it was monitored in real-time with on-line displays. Once the periodic state was reached, the gas phase concentration bed profiles measured by the autosampling system were obtained in triplicate over a period of three cycles. Also, the heavy and light (if breakthrough occurred) product effluent concentration histories, feed concentration, and pure butane (as a standard) were measured manually using gas-tight syringes and the same GC. The effluent concentration histories were sampled under both positive and negative gauge pressures using gas-tight syringes. Typically, nine to eleven samples were taken during each of the blowdown and purge steps. The light product purity was also obtained from the GC in a similar fashion using the gas-tight syringes under positive pressure.

After one series of runs were completed, the PSA process was stopped and the beds were regenerated as specified above. After the columns were cooled down, the next series of runs commenced. This procedure was repeated until all of the runs were completed. During each series of runs an attempt was also made to fix all of the parameters except for the one being investigated.

This included the pressure histories, where in each run the pressurization rate was adjusted so that feed pressure was reached by the end of Step I. An attempt was also made to control the blowdown rate so that the purge pressure was reached by the end of Step IV. In this way the pressure histories associated with each series of runs (the only manually controlled parameter) were forced to exhibit similar trends.

RESULTS AND DISCUSSION

Twenty-four experiments divided into six series were carried out using the unique PSA–SVR system to study the transient and periodic dynamic behavior of the nitrogen–butane vapor–BAX activated carbon system. Table 2 gives

TABLE 2
PSA–SVR Process Conditions[a]

Run	V_f (SLPM)	γ (—)	y_f (%)	t_c (min)	t_{pb} (min)	P_L (kPa)
A1	2.5	*1.41*	*21.2*	20	2	*14.7*
A2	2.5	*1.28*	20.8	20	2	13.5
A3	2.5	*1.14*	21.8	20	2	12.2
A4	2.5	*0.50*	20.4	20	2	13.7
A5	2.5	*0.24*	20.8	20	2	14.6
B1	2.5	1.45	19.9	20	2	*28.3*
B2	2.5	1.49	20.3	20	2	*41.4*
B3	2.5	1.48	19.6	20	2	*55.7*
B4	2.5	1.50	20.4	20	2	*68.8*
C1	*1.5*	1.48	19.7	20	2	13.9
C2	*2.5*	1.50	20.9	20	2	13.8
C3	*3.5*	0.86	20.6	20	2	23.9
C4	*4.0*	0.80	20.6	20	2	26.5
D1	2.5	1.41	*9.5*	20	2	14.6
D2	2.5	1.17	*31.4*	20	2	17.6
D3	2.5	0.94	*39.3*	20	2	22.0
E1	2.5	0.74	34.0	*10*	1.0	27.7
E2	2.5	0.73	34.9	*15*	1.5	28.3
E3	2.5	0.69	35.8	*20*	*2.0*	29.8
E4	2.5	0.73	35.3	*25*	2.5	28.4
E5	2.5	0.76	35.6	*30*	3.0	26.9
F1	2.5	0.76	34.5	26	*5*	27.2
F2	2.5	0.75	34.9	24	*4*	27.3
F3	2.5	0.74	34.4	22	*3*	27.8

[a] The adsorption (Step II) pressure for all runs was approximately 151.6 kPa.

the process conditions of each run. The italicized values in each numerical column in Table 2 correspond to a series of runs.

Periodic State Verification and Multiplicity

Attainment of the periodic state was judged by the constancy of the temperature from cycle to cycle. In all of the runs the temperatures were monitored at the end of the adsorption step of each cycle at the nine axial positions in the bed. These temperatures were recorded by the DAC system and displayed on screen as a function of the cycle number. When each of these curves exhibited a horizontal line, the periodic state was reached. As a verification of the periodic state, the concentration profiles in the bed at the beginning and end of the adsorption step were obtained repeatedly over numerous cycles. The results agreed remarkably well in all cases. As an example of the approach to the periodic state in one of the experimental runs, Fig. 2 displays the actual temperature versus cycle plot at the end of Step II for the run starting from clean beds, but at the same conditions as E3. For this run the periodic state

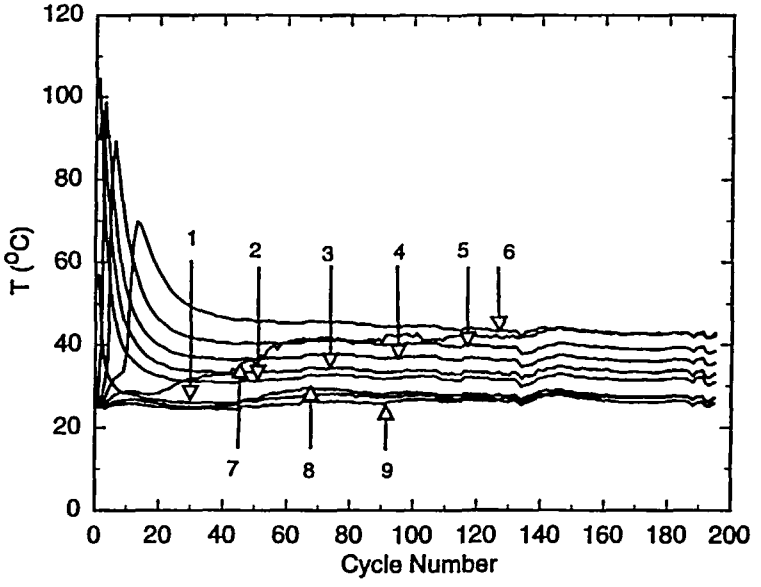

FIG. 2 Temperature histories as a function of the cycle number at the end of the adsorption step at different positions in the bed, showing the approach to the periodic state for Run E3 that started from clean beds. Numbers 1 to 9 represent the positions of z/L = 0.08, 0.185, 0.29, 0.395, 0.5, 0.605, 0.71, 0.815, and 0.92, respectively.

was reached in approximately 143 cycles, as indicated by the leveling off of the nine temperature profiles.

In this experimental study each series of runs was also started from clean beds, and the process conditions were chosen such that the first run resulted in the smallest bed penetration. Subsequent runs in the series were started from beds at the periodic state of the previous run. So it was of interest to verify whether the periodic state of the intermediate run was the same as that when starting from clean beds. Several intermediate runs (Runs A2, B3, C3, E3, and F3) were repeated at the same conditions, except that they were started from clean beds. Essentially the same periodic state was reached for each pair of runs, independent of the initial condition of the bed. The intermediate Run E3 was selected as an example to illustrate the uniqueness of the periodicity. Figure 3(a) compares the butane vapor concentration profiles at the beginning and end of the adsorption step, and Fig. 3(b) compares the temperature profiles at the end of each step for intermediate Run E3 and an identical run that was started from clean beds.

The temperature profiles for these two runs were almost exactly the same. The 1 to 2°C differences were caused by slight differences in the feed and ambient temperatures. The butane vapor concentration profiles were even more convincing, being almost identical for these two runs, especially at the beginning of the adsorption step. These results demonstrated very well that the periodic states of these two runs were the same; results from the other runs that were repeated were equally convincing. These results also suggested that a PSA–SVR process starting from partially contaminated beds approaches the same periodic state as that starting from clean beds, as long as the final periodic state corresponds to beds more contaminated than the initial condition of the beds.

Transient Process Dynamics

Figure 2 shows the slow, transient approach to the periodic state which was observed most clearly at $z/L = 0.71$ (7th position). At this position and at the end of the adsorption step of each cycle, the gradual increase in temperature from ambient to about 42°C was indicative of the slowly progressing temperature and concentration wave fronts, which apparently never reached $z/L = 0.82$ (8th position). The 8th and 9th positions remained essentially at ambient conditions throughout the experiment. In contrast, all of the positions below the 7th position exhibited very sharp increases in temperature, where each position eventually leveled off at its unique periodic state temperature.

At the end of the 1st cycle, the 1st position experienced the highest temperature, which peaked at about 105°C and then rapidly decreased to near ambient conditions after about 10 cycles. This marked temperature rise was associated

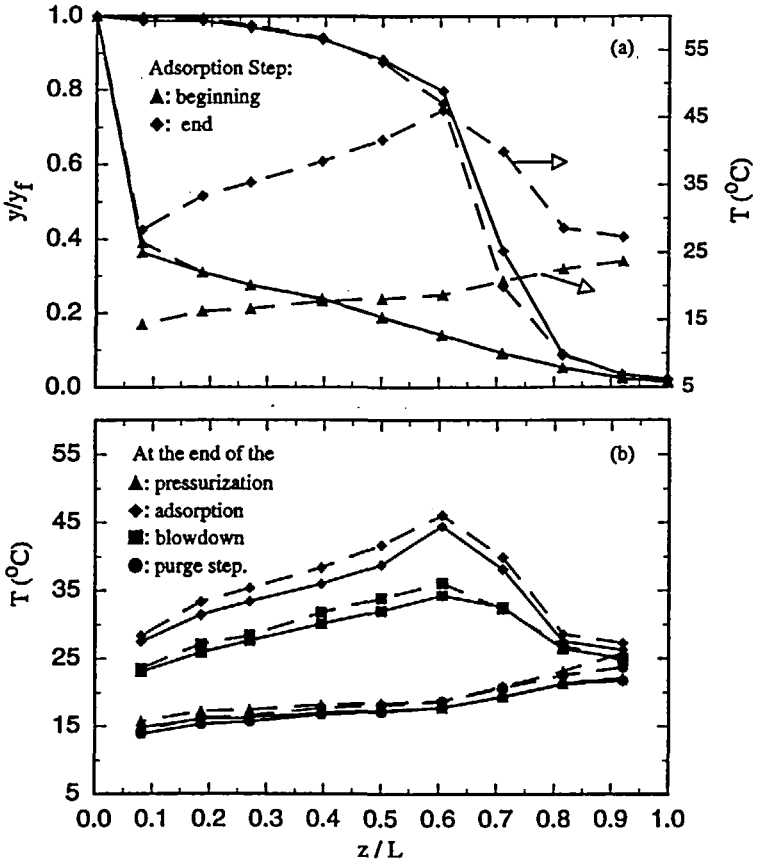

FIG. 3 Periodic state bed profiles of Run E3. Dashes represent the results of the run starting from the periodic state of Run E2; solid lines represent the results of the run starting from clean beds; (a) concentration and temperature profiles at the beginning and end of the adsorption step; and (b) temperature profiles at the end of each step.

with the adsorption of 35 vol% butane vapor in nitrogen on a clean carbon bed. However, as the number of cycles increased, the 1st position became more contaminated until it became completely saturated with the feed at the end of Step II, as evidenced by the near ambient temperature exhibited at this position after 10 cycles. In time, the temperature wave progressed toward the light product end of the bed, with increasing higher positions in the bed experiencing the peak temperatures. But of course, all of these peak temperatures dampened in time as the periodic state was approached.

At the end of 15th cycle the peak temperature was only about 70°C, and the temperature wave reached the 6th position. After about 40 cycles the process became very close to the periodic state at all positions except for the 7th position (z/L = 0.71); and now the approach to the periodic state slowed, as indicated by the very gradual movement of the temperature wave at the 7th position. It took about 143 cycles for the process to reach the periodic state, where the peak temperatures, located at the 6th and 7th positions (z/L = 0.61 and 0.71), were only about 42°C. At the periodic state the portion of the bed from z/L = 0.82 to the light product end was only slightly contaminated with butane, as evidenced by the constant (near ambient) temperatures at the 8th and 9th positions (z/L = 0.815 and 0.92) and the small butane vapor concentrations in the light product stream (28).

Figure 4 displays the same information as Fig. 2 for Run E3, but this time Run E3 started from partially contaminated columns, i.e., columns initially at the periodic state of Run E2. It took about 60 cycles to reach the periodic state after switching the process conditions from Run E2 to Run E3, as evidenced by the leveling off of the profile at the 7th position (z/L = 0.71).

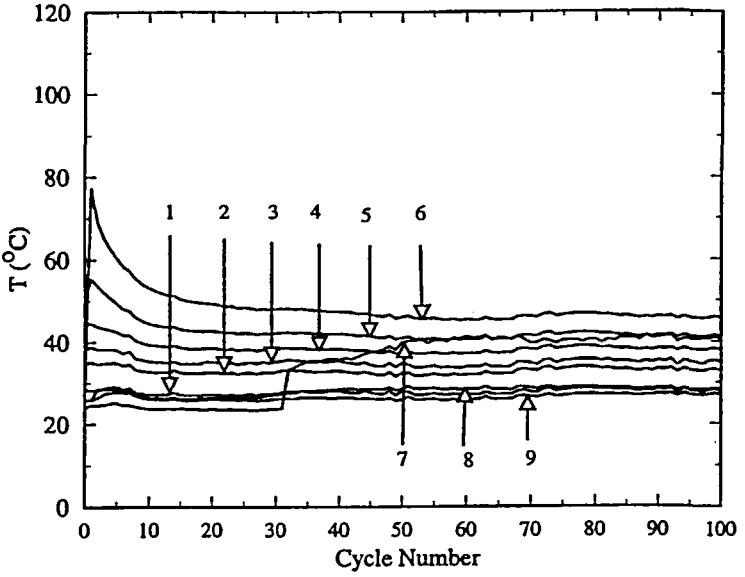

FIG. 4 Temperature histories as a function of the cycle number at the end of the adsorption step at different positions in the bed for Run E3 that started from the initial condition of the periodic state of Run E2, showing the approach to the periodic state. Numbers 1 to 9 represent the positions of z/L = 0.08, 0.185, 0.29, 0.395, 0.5, 0.605, 0.71, 0.815, and 0.92, respectively.

This time was less than half of that taken to reach the periodic state when starting from clean beds. After switching the process conditions (1st cycle in Fig. 4), the 5th and especially the 6th positions experienced sharp increases in temperature, from 49°C at the periodic state of Run E2 to 55°C, and from 25°C at the periodic state of Run E2 to 77°C, respectively. This result demonstrated the quick movement of the mass transfer zone (MTZ) during the initial transient period. Afterward the temperatures at these two positions decreased slowly with increasing cycle number as they approached the periodic state. The temperatures from the 1st to the 4th positions hardly changed during the transient period because these positions were already saturated at the conditions associated with the end of adsorption step before switching from Run E2 to Run E3. The temperature at the 7th position ($z/L = 0.71$) also remained the same until about the 31st cycle, when a sudden increase in temperature occurred followed by a very gradual increase until the periodic state was reached after about 60 cycles. This result demonstrated the very slow movement of the MTZ after the initial transient period. The temperature profiles at the end of the adsorption and purge steps plotted in Fig. 3(a) also show that the concentration and temperature fronts essentially tracked each other. This was a general result observed in all of the runs of this study. It was also an important result because it indicated that temperature front sensing can be used to track the position of the concentration wave front, similarly to that proposed for PSA air separation (29).

The high transient temperatures at the 6th position (about 52°C above the periodic state temperature of the previous run), exhibited just after switching from Run E2 to Run E3, indicated that very slight changes in process conditions (like the feed flow rate, feed concentration, etc.) can cause significant temperature increases in the bed. This result lends considerable insight into the usual practice of preconditioning the beds prior to full operation in order to avoid excessive temperature rises (30). If the preconditioning results in beds less contaminated than at the periodic state, high transient temperatures can be expected during the initial cycles of full operation. If the preconditioning results in beds more contaminated than the periodic state, the high transient temperatures can be avoided, but possibly at the expense of deteriorating the periodic process performance. For example, allowing the slowly moving MTZ to cover more of the bed could foster unnecessary breakthrough of solvent vapor into the light product. Nevertheless, some preconditioning is needed to avoid the exceedingly high temperatures exhibited when starting a process with virgin carbon, as shown in Fig. 2. For example, under similar circumstances except for the initial condition of the beds, virgin carbon resulted in an 80°C rise in temperature peaking at 105°C (Fig. 2), whereas a partially contaminated carbon resulted in a 52°C rise in temperature peaking only at 77°C.

Figure 5 shows the transient temperature profiles at the end of each step for Run A1 (see Table 2), which started from clean beds and reached the periodic state after about 80 cycles. The differences between the transient and periodic state temperature profiles, along with the temperature changes, were quite drastic. The highest temperature occurred at the end of the adsorption step of the 1st cycle at the 2nd position ($z/L = 0.185$) (Fig. 5b), which peaked at about 95°C, whereas the lowest temperature reached about 10°C at the end of the purge step of the periodic state at the 1st position ($z/L = 0.08$) (Fig. 5d). As the periodic state was approached, however, the peak temperatures decreased and moved cocurrently in the axial direction with increasing cycle number. These results showed that significant transient temperature rises occurred over large portions of the bed, exceeding 75°C during the first five cycles. These temperature rises were indicative of the slowly migrating MTZ which covered only 50% of the bed at the period state (28). So large potentially dangerous temperature excursions can be exhibited in PSA–SVR systems over large fractions of the bed, but only during the initial cycles of operation from start-up.

A comparison of the temperature profiles at the end of various process steps showed that pressurization did not have much effect on the temperature profiles, which was consistent with simulation results in the literature (11). However, the other three steps did have a significant effect. For example, during the 1st cycle, the peak temperature increased from 38°C at the end of the pressurization step ($z/L = 0.185$ in Fig. 5a) to about 95°C at the end of the adsorption step ($z/L = 0.185$ in Fig. 5b), the peak temperature decreased from 95°C at the end of adsorption step to about 65°C at the end of the blowdown step (Fig. 5c), and the temperature decreased even further from 65°C at the end of the blowdown step to about 38°C at the end of the purge step. In contrast, the periodic state peak temperatures shifted to $z/L = 0.29$ and the effects of each step were significantly less pronounced.

Figure 6 shows the same information as in Fig. 5 but for Run D1 which also started from clean beds and differed from Run A1 only by the feed concentration (9.5 vol% in Run D1 compared to 21.2 vol% in Run A1, see Table 2). The transient and periodic state temperature profiles were similar between these two runs; however, the lower feed concentration produced significantly lower transient and periodic state temperature rises. The highest transient temperature occurred at the 2nd position of the 2nd cycle at the end of the adsorption step, which peaked at about 67°C and was about 30°C lower than that in Run A1. These results offered considerable insight into how to precondition the beds prior to full operation, e.g., by using fairly dilute feed concentrations.

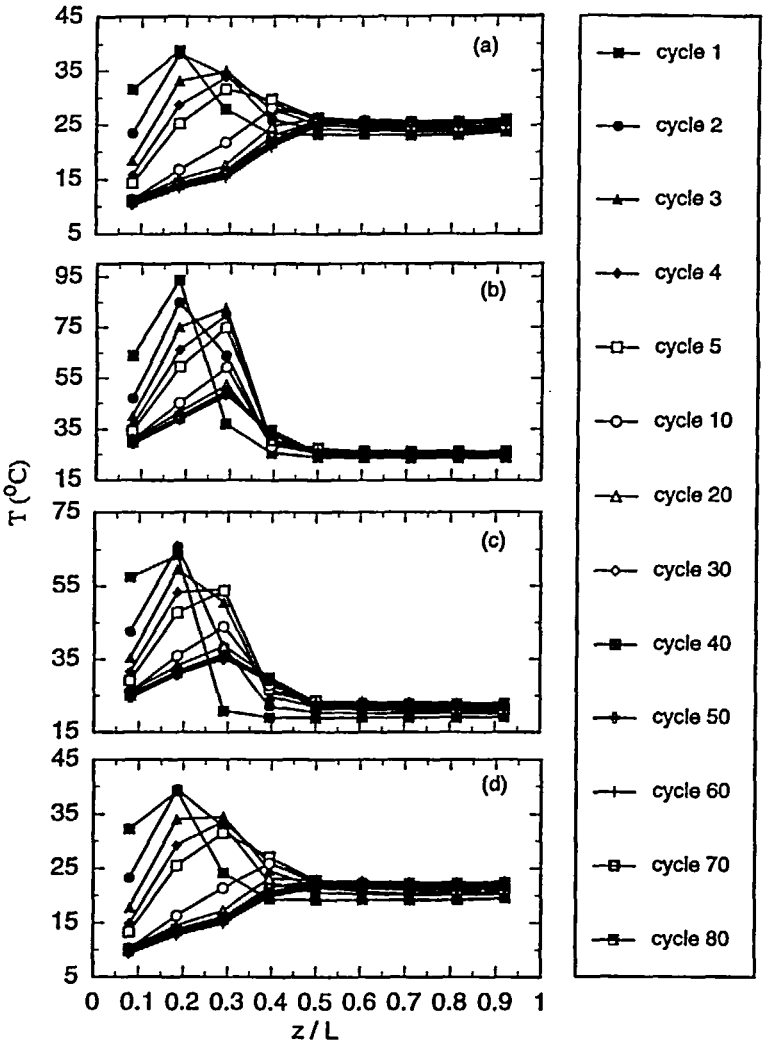

FIG. 5 Transient bed temperature profiles showing the gradual approach to the periodic state for Run A1 at the end of the (a) pressurization, (b) adsorption, (c) blowdown, and (d) purge steps.

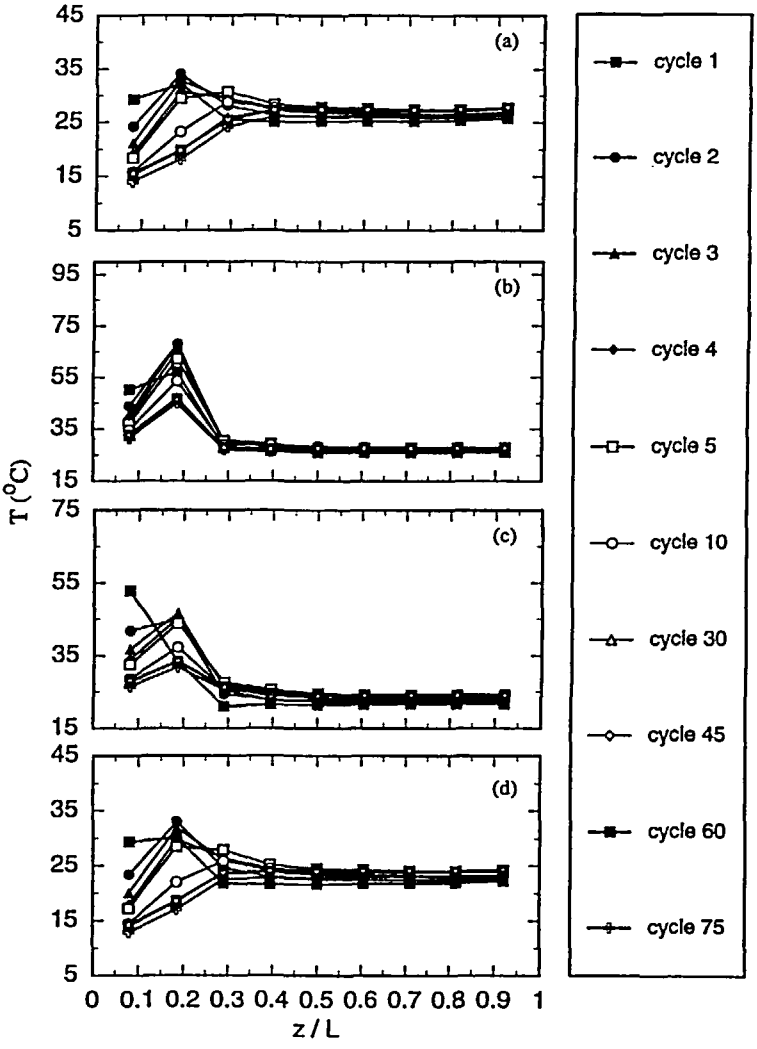

FIG. 6 Transient bed temperature profiles showing the gradual approach to the periodic state. for Run D1 at the end of the (a) pressurization, (b) adsorption, (c) blowdown, and (d) purge steps.

Periodic State Process Dynamics

Run A1 was chosen as an example to illustrate the periodic state process dynamics. Figure 7(a) displays a typical representation of the periodic state pressure histories of all the experimental runs. Subtle differences between the pressure histories for each set of runs are presented in Part II (28). Remember that these pressure histories were manually adjusted, and in some cases the profile shape during purge was constrained by the inherent system resistances. So not all of the pressure histories were exactly the same in each series of runs.

Figure 7(b) displays the column outer surface and ambient temperatures during a periodic state cycle. The thermocouple used to measure the surface temperature of the column was placed on the axial center of the column outer surface. The temperature of the column outer surface did not change much during the whole cycle and stayed very close to the ambient temperature. Considering the large temperature swings that occurred inside the column, this suggested that the overall heat transfer resistance of the column was quite large, and that the system operated close to the adiabatic condition.

Figure 7(c) shows the periodic temperature variations of the first four positions from the feed inlet of the column. Pressurization (Region I) hardly changed the temperatures of the contaminated regions of the bed, though very slight increases occurred. During the adsorption step (Region II), the temperature wave propagated to the light product end of the bed at essentially a constant velocity (the 1st to the 9th positions were equally spaced), indicative of the movement of the concentration wave front. The peak temperature also increased as the temperature wave progressed through the bed because the positions farther from the feed inlet were less contaminated, which led to more adsorption of butane vapor and hence more heat released. At the end of the adsorption step, the highest temperature was located at the 3rd position ($z/L = 0.29$). This was also indicative of the location of the butane vapor concentration wave front, since in this kind of system the temperature and concentration waves usually tracked each other as suggested earlier and in the literature (11, 22, 29). The tail of the concentration wave front reached the 4th position ($z/L = 0.395$) as evidenced by the temperature increase at this position at the end of the adsorption step. Blowdown (Region III) decreased the bed temperatures, and purge (Region IV) led to further decreases. The relatively large temperature drop that occurred during the blowdown step was indicative of a large amount of butane desorbing. This result was different from that reported in the literature for the benzene-activated charcoal system (11), where hardly any temperature drop was observed during this step, perhaps because of the differences in the adsorption isotherms. The temperature at the wave front region (around the 3rd position) also exhibited the largest

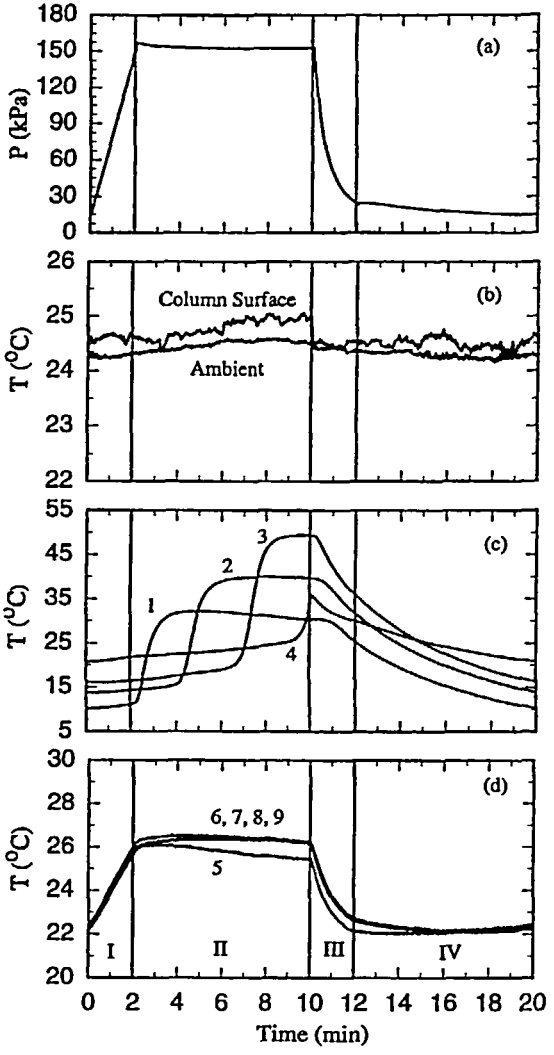

FIG. 7 Pressure and temperature histories during a complete periodic state cycle of Run A1: (a) pressure; (b) ambient and column outer-surface temperatures; and (c) and (d) column centerline temperatures. Numbers 1 to 9 represent the positions of z/L = 0.08, 0.185, 0.29, 0.395, 0.5, 0.605, 0.71, 0.815, and 0.92, respectively.

decrease, again indicating that a large amount of butane desorbed in this region.

Figure 7(d) displays the temperature variations from the 5th to the 9th positions during the same periodic cycle. These positions were essentially uncontaminated except for the 5th position, where traces of butane vapor probably reached. The periodic state temperature swings associated with the 6th to the 9th positions were caused by the carrier gas (nitrogen) adsorbing during pressurization and desorbing during blowdown. They were not caused by compression and expansion effects, because according to the pressurization region of Fig. 7(c), these effects amounted to less than a 1°C change. This result was in agreement with that reported in the literature (11), where it was shown that the compression/expansion effects are minimized due to the presence of the adsorbent.

Figure 8 displays the butane vapor concentration histories in the light product stream during the adsorption step (y_p) but only for the series of runs which exhibited butane vapor breakthrough in some or all of the runs. In general, the butane vapor mole fraction in the light product increased with time during the feed step in a manner that was characteristic of dispersed wave breakthrough behavior, i.e., it was uncharacteristic of the breakthrough behavior associated with a highly favorable adsorption isotherm. Similar dynamic dispersed wave breakthrough behavior was reported elsewhere in a PSA air purification process (7, 8). Increasing the volumetric flow rate (Fig. 8b) and cycle time (Fig. 8c), as well as decreasing the volumetric purge-to-feed ratio (Fig. 8a) and pressurization/blowdown time (Fig. 8d), all caused the butane vapor mole fraction in the light product to increase; however, the increases of the butane vapor mole fraction in the light product caused by decreasing the pressurization/blowdown time were trivial.

Figure 9 displays the butane vapor concentration histories at the exit of the bed during the blowdown and purge steps (y_e) for all of the runs. In general, the effluent concentration increased rapidly during the blowdown step, and at the end of this step it reached a maximum or a plateau. This trend was different from that reported for the benzene-activated charcoal system (11), where the recovered butane vapor concentration increased slowly at first but then very rapidly near the end of the blowdown step. This difference was associated with the stronger affinity between the adsorbate and adsorbent in the benzene-activated charcoal system, which made the benzene-activated charcoal system more representative of an ideal system, i.e., the behavior of the effluent concentration (y_e) was more like that described by the frozen-solid-phase assumption (9, 10, 31).

During the purge step the effluent concentration at the beginning of the step, in general, decreased quickly and then gradually until the end of the purge step. The initial rapid decrease was caused by the introduction of the

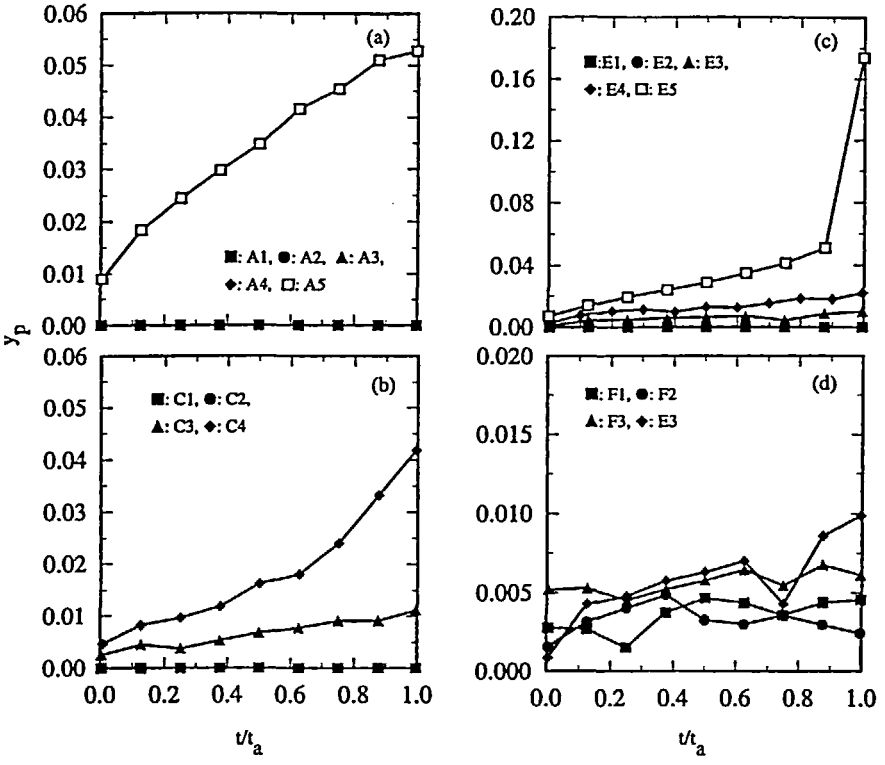

FIG. 8 Butane vapor concentration histories in the light product stream during the adsorption step, showing the effects of the (a) purge-to-feed ratio, (b) volumetric flow rate, (c) cycle time, and (d) pressurization/blowdown step time. The letters and numbers correspond to those given in Table 2.

purge gas and its dilution effect. The extent of this decrease depended on the process conditions, especially the volumetric purge-to-feed ratio (γ), but also the purge pressure (P_L) and the feed volumetric flow rate (V_f) that are directly related to the purge-to-feed ratio (11, 28).

According to Fig. 9(a), for a volumetric purge-to-feed ratio of 1.41 (Run A1), the initial decrease in the effluent concentration with time was the quickest; but for a volumetric purge-to-feed ratio of 0.24 (Run A5), the effluent concentration was almost constant during the purge step because of the small amount of purge gas that was used and thus there was less dilution effect. A small purge-to-feed ratio also resulted in a higher effluent concentration during the blowdown step since it led to a larger portion of the bed being contami-

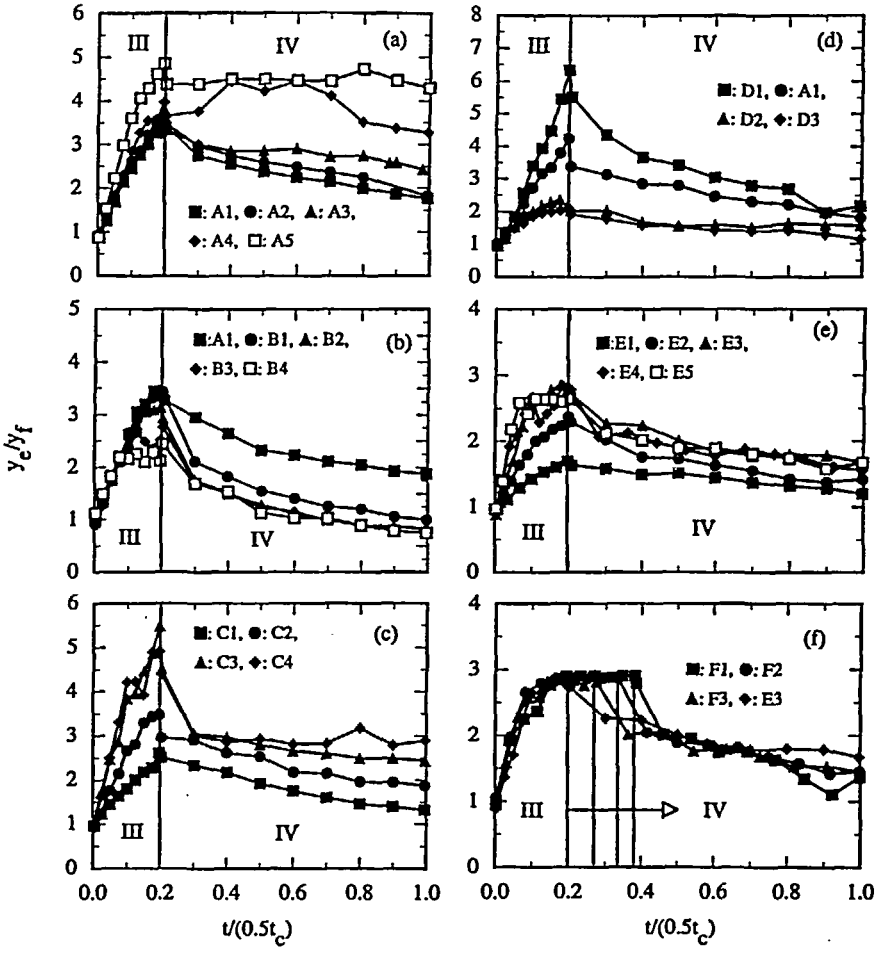

FIG. 9 Effluent histories during the blowdown (III) and purge (IV) steps, showing the effects of the (a) purge-to-feed ratio, (b) purge pressure, (c) volumetric feed flow rate, (d) feed concentration, (e) cycle time, and (f) pressurization/blowdown step time. The letters and numbers correspond to those given in Table 2.

nated during the adsorption step and thus more desorption during the blowdown step. Similarly, a lower purge pressure and volumetric feed flow rate both led to higher effluent concentrations (Figs. 9b and 9c) because less purge gas was used at a constant purge-to-feed ratio. However, attention must be paid to the feed concentration (y_f) effect (Fig. 9d). A lower feed concentration

led to higher ratios of the effluent-to-feed concentrations, but not necessarily higher effluent concentrations (y_c). Figure 9(e) shows that the cycle time (t_c) effect on the effluent concentration was even more complex. Increasing the cycle time from 10 to 25 minutes (Runs E1 to E4) increased the effluent concentrations; but further increasing the cycle time from 25 to 30 minutes (Runs E4 to E5) decreased the effluent concentrations. A detailed explanation of this phenomenon is offered in Part II (28). Figure 9(f) shows that even for the shortest pressurization/blowdown step time (2 minutes), the effluent was comprised of almost pure butane vapor (98.1 vol%) at the end of the blowdown step; and further increases in the pressurization/blowdown step time increased the duration during which this highly concentrated butane stream was produced (e.g., Run F1). But the effluent concentrations during the purge step counteracted this effect. So the time-averaged effluent concentration for each run in this series did not change significantly as shown in Part II (28). Nevertheless, the unique profiles that resulted when increasing the pressurization/blowdown step time (Fig. 9f) suggested that it may be possible to improve the enrichment of the butane by modifying the cycle; this is also discussed in Part II (28).

CONCLUSION

A unique PSA–SVR system was used to investigate the transient and periodic process dynamics associated with recovering butane vapor from nitrogen using Westvaco BAX activated carbon. Marked differences between the transient and periodic thermal waves were observed. In most of the 24 runs the approach to the periodic state was very slow, taking up to 160 cycles or more, depending on the process conditions. When the process was started from clean beds, transient peak temperatures within the bed reached two to three times higher than those at the periodic state, depending on the process conditions. Even when the process was started from partially contaminated beds, transient peak temperatures were still very high as long as the new periodic state resulted in more adsorbent being contaminated. In both cases, however, the high transient temperatures quickly decreased and approached the periodic temperatures within only a few cycles. Also, when starting the process from partially contaminated beds, the same periodic state was approached as that starting from clean beds as long as the approach to the periodic state resulted in a progressively more contaminated bed. These facts suggested that the practice of preconditioning beds to avoid high transient temperatures may be futile, depending on the extent of preconditioning.

Pressurization did not cause significant changes in the temperature profiles compared to the large transient and periodic state temperature swings (35 to 45°C) resulting from adsorption and desorption. The adsorption step was

responsible for the temperature increases; and contrary to results in the literature, blowdown significantly contributed to the temperature decrease, though the major decreases occurred during the purge step. Compression and expansion effects were negligible in this system, which was in agreement with that reported in the literature for a PSA–air purification process.

At the periodic state the enriched butane vapor concentration effluent history usually rapidly increased during blowdown and reached a maximum or plateau at the end of this step. This behavior indicated that the butane-activated carbon system was far removed from the ideal conditions associated with the frozen-solid-phase assumption and strong adsorbate systems. During the purge step, the butane vapor concentrations generally decreased with time because of the dilution effect of the purge gas. However, depending on the purge-to-feed ratio or other process parameters related directly to the purge-to-feed ratio, such as the purge pressure and volumetric flow rate, the effluent concentration essentially remained constant during the purge step, or it even increased with time, leading to a higher enrichment. The periodic blowdown and purge step effluent histories also gave considerable insight into new cycle designs for obtaining higher vapor enrichments.

NOMENCLATURE

L	bed length (m)
P	pressure (kPa)
T	temperature (°C)
t	time (minutes)
V	volumetric flow rate (SLPM/s)
y	gas-phase mole fraction
z	axial position (m)

Greek Symbols

γ	purge-to-feed ratio

Subscripts

c	cycle
e	effluent
f	feed
H	high
L	low
pb	pressurization and blowdown
I, II, III, IV	step numbers

ACKNOWLEDGMENTS

The authors gratefully acknowledge financial support from the National Science Foundation under Grant CTS-9410630, and from the Westvaco Charleston Research Center.

REFERENCES

1. D. M. Ruthven, *Principles of Adsorption and Adsorption Processes*, Wiley, New York, NY, 1984.
2. R. T. Yang, *Gas Separation by Adsorption Process*, Butterworth, London, 1986.
3. M. Suzuki, *Adsorption Engineering*, Elsevier, Tokyo, 1990.
4. D. M. Ruthven, S. Farooq, and K. S. Knaebel, *Pressure Swing Adsorption*, VCH Publishers, New York, NY, 1994.
5. D. J. Pezolt, S. J. Collick, H. A. Johason, and L. A. Robbins, "Pressure Swing Adsorption for VOC Recovery at Gasoline Loading Terminals," *Environ. Prog.*, *16*(1), 16–19 (1997).
6. R. J. Holman and J. H. Hill, *New Developments in Hydrocarbon Vapor Recovery*, Paper presented at AIChE 1992 Annual Meeting, Miami Beach, FL, November 1–6, 1992.
7. J. A. Ritter and R. T. Yang, "Pressure Swing Adsorption: Experimental and Theoretical Study on Air Purification and Vapor Recovery," *Ind. Eng. Chem. Res.*, *30*, 1023–1032 (1991).
8. J. A. Ritter and R. T. Yang, "Air Purification and Vapor Recovery by Pressure Swing Adsorption: A Comparison of Silicalite and Activated Carbon," *Chem. Eng. Commun.*, *108*, 289–305 (1991).
9. D. Subramanian and J. A. Ritter, "Equilibrium Theory for Solvent Vapor Recovery by Pressure Swing Adsorption: Analytical Solution for Process Performance," *Chem. Eng. Sci.*, *52*, 3161–3172 (1997).
10. Y. Liu and J. A. Ritter, "Evaluation of Model Approximations in Simulating Pressure Swing Adsorption-Solvent Vapor Recovery," *Ind. Eng. Chem. Res.*, *36*, 1767–1778 (1997).
11. Y. Liu and J. A. Ritter, "Pressure Swing Adsorption-Solvent Vapor Recovery: Process Dynamics and Parametric Study," *Ibid.*, *35*, 2299–2312 (1996).
12. Y. Liu and J. A. Ritter, "Fractional Factorial Study of a Pressure Swing Adsorption-Solvent Vapor Recovery Process," *Adsorption*, *3*, 151–163 (1997).
13. Y. Liu and J. A. Ritter, "Periodic State Heat Effects in Pressure Swing Adsorption-Solvent Vapor Recovery," *Ibid.*, *4*, 159–172 (1998).
14. E. S. Kikkinides and R. T. Yang, "Simultaneous SO_2/NO_x Recovery from Flue Gas by Pressure Swing Adsorption," *Ind. Eng. Chem. Res.*, *30*, 1981–1989 (1991).
15. D. K. Friday and M. D. LeVan, "PSA for Air Purification: Experiments and Modeling," in *Fundamentals of Adsorption* (M. Suzuki, Ed.), Elsevier, Tokyo, 1992, pp. 17–22.
16. E. S. Kikkinides, V. I. Sikavitsas, and R. T. Yang, "Natural Gas Desulfurization by Adsorption: Feasibility and Multiplicity of Cyclic Steady States," *Ind. Eng. Chem. Res.*, *34*, 255–262 (1995).
17. K. Chihara and M. Suzuki, "Simulation of Nonisothermal Pressure Swing Adsorption," *J. Chem. Eng. Jpn.*, *16*, 53 (1983).
18. D. Psaras, G. Leach, and A. I. LaCava, "Experimental Study of Transient Thermal Effects on a Model Pressure Swing Adsorption Process," in *Adsorption and Ion Exchange: Funda-*

mentals and Applications (*AIChE Symposium Series, Vol. 84*) (M. D. LeVan, Ed.), AIChE, New York, NY, 1988, pp. 133–140.
19. D. M. Ruthven and S. Farooq, "Concentration of a Trace Component by Pressure Swing Adsorption," *Chem. Eng. Sci.*, *49*, 51–60 (1994).
20. R. T. Yang and S. J. Doong, "Gas Separation by Pressure Swing Adsorption: A Pore-Diffusion Model for Bulk Separation," *AIChE J.*, *31*, 1829–1842 (1985).
21. S. J. Doong and R. T. Yang, "Bidisperse Pore Diffusion Model for Zeolite Pressure Swing Adsorption," *Ibid.*, *33*, 1045–1049 (1987).
22. P. Cen and R. T. Yang, "Bulk Gas Separation by Pressure Swing Adsorption," *Ind. Eng. Chem. Fundam.*, *25*, 758 (1986).
23. A. Kapoor and R. T. Yang, "Separation of Hydrogen-Lean Mixtures for a High-Purity Hydrogen by Vacuum Swing Adsorption," *Sep. Sci. Technol.*, *23*, 153–178 (1988).
24. S. J. Doong and R. T. Yang, "Bulk Separation of Multicomponent Gas Mixtures by Pressure Swing Adsorption: Pore/Surface Diffusion and Equilibrium Models," *AIChE J.*, *32*, 397–410 (1986).
25. P. Cen, W. Chen, and R. T. Yang, "Ternary Gas Mixture Separation by Pressure Swing Adsorption: A Combined Hydrogen-Methane Separation and Acid Gas Removal Process," *Ind. Eng. Chem., Process Des. Dev.*, *24*, 1201–1208 (1985).
26. P. Cen and R. T. Yang, "Separation of a Five-Component Gas Mixture by Pressure Swing Adsorption," *Sep. Sci. Technol.*, *20*, 725–747 (1985).
27. E. D., Tolles, Westvaco Charleston Research Center, Charleston, Personal Communication, 1996.
28. Y. Liu, C. E. Holland, and J. A. Ritter, "Solvent Vapor Recovery by Pressure Swing Adsorption. II. Experimental Periodic Performance of the Butane-Activated Carbon System," *Sep. Sci. Technol.*, In Press.
29. M. J. Matz and K. S. Knaebel, "Temperature Front Sensing for Feed Step Control in Pressure Swing Adsorption," *Ind. Eng. Chem. Res.*, *26*(8), 1638 (1987).
30. B. K., Kaul, Exxon Research and Engineering Company, Florham Park, Personal Communication, 1997.
31. M. D. LeVan, "Pressure Swing Adsorption: Equilibrium Theory for Purification and Enrichment," *Ind. Eng. Chem. Res.*, *34*, 2655–2600 (1995).

Received by editor September 2, 1997
Revision received April 1998